ADVANCED FUNCTIONAL MATERIALS
www.afm-journal.de
www.MaterialsViews.com

TiO_2 Microspheres with Controllable Surface Area and Porosity for Enhanced Light Harvesting and Electrolyte Diffusion in Dye-Sensitized Solar Cells

Yong Ding, Li Zhou, Li'e Mo, Ling Jiang, Linhua Hu, Zhaoqian Li, Shuanghong Chen, and Songyuan Dai**

An optimized configuration of TiO_2 microspheres in photoanodes is of great importance to prepare highly efficient dye-sensitized solar cells (DSSCs). In this work, TiO_2 microspheres with tunable diameter, pore size, and porosity are synthesized by subtly adjusting the synthesizing conditions, including ratios of deionized water, ammonia, and ethanol, respectively. TiO_2 microspheres are obtained with large pore sizes and a high porosity without sacrificing specific surface areas. In addition, the effect of their porosity and pore size on the performance of DSSCs is investigated. As confirmed by the dye-loading ability and electrolyte diffusion resistance, the large mesopores and the high porosity of the TiO_2 microspheres can improve dye adsorption and facilitate electrolyte diffusion, giving rise to a high light-harvesting and electron collection efficiency. Consequently, the highest photocurrent of 19.21 mA cm^{-2} and a power conversion efficiency of 9.98% are obtained by using the TiO_2 microspheres with the highest porosity, compared with a 9.29% efficiency demonstrated by the lowest porosity (an improvement of 7.4%). By modifying the interconnection and the external pores of the microspheres photoanode, a high efficiency of 11.67% is achieved for a DSSC based on the most potent TiO_2 microspheres.

1. Introduction

Dye-sensitized solar cells (DSSCs) have aroused extensive interest as a promising alternative to conventional silicon-based solar cells because of its high-efficiency and low-cost photovoltaic devices.[1] For an efficient DSSC, the photoanode must simultaneously meet the following several requirements: (1) high specific surface area for abundant dye adsorption; (2) superior light scattering for improved light harvesting; (3) prominent electron transport and recombination for frequent electron collection; and (4) suitable pore sizes and porosities for sufficient electrolyte diffusion.[2,3] Whereas, these requirements are more often than not incompatible with one another in the one nanomaterial.

TiO_2 microspheres are one of the most successful nanomaterials for satisfying the above requirements.[4–6] Despite the vast reports on the synthesis of TiO_2 microspheres, major challenges are still existed in the precise control over the morphology, specific surface area, diameter, and pore size in a facile scalable preparation.[7–12] Understanding those properties of TiO_2 microspheres is devoted to develop high-performance DSSCs.[5] Chen et al. have studied the effect of mesoporous TiO_2 bead diameter on the efficiency of DSSCs.[9] They found that 320 ± 50 nm beads have the highest dye adsorption and 550 ± 50 nm beads own the highest light scattering. Effect of pore sizes on the mass transport for cobalt-based redox couples was also researched by Grätzel et al.[13] It is interesting to note that the large external pores provide a high-speed channel for unhindered electrolyte diffusion. Additionally, an efficient light scattering and a high internal surface area are synchronously achieved in this large porous structure. Whereas, the associated increase in pore sizes via increasing the amount of ammonia in the solvothermal treatment is accompanied by the decrease of specific surface area.[10,13] But beyond that, varying the ratio of ethyl cellulose to TiO_2 in the paste or optimizing the $TiCl_4$ post-treatment is commonly used to adjust the pore size and porosity of the mesoporous photoanode.[14] Although the porosity is increased from 0.52 to 0.59, the dye loading is decreased by 23%. Therefore, it is still a significant goal to synthesis large pore size and high porosity of microspheres without sacrificing the specific surface area. Here, we propose a facile approach to solve this problem.

In the first part, we have synthesized TiO_2 microspheres with a tunable diameter and pore size by altering the experiment condition, such as the amount of deionized water and ammonia, respectively. By studying comparatively the light scattering, specific surface area, and pore size, we have obtained TiO_2 micro-

Dr. Y. Ding, Dr. L. Zhou, Dr. L. Mo, Dr. L. Jiang, Prof. L. Hu, Dr. Z. Li, Dr. S. Chen, Prof. S. Dai
Key Laboratory of Novel Thin-Film Solar Cells
Institute of Applied Technology
Hefei Institutes of Physical Science
Chinese Academy of Sciences
Hefei, Anhui 230031, P. R. China
E-mail: solarhu@sina.com; sydai@ipp.ac.cn
Prof. S. Dai
Beijing Key Laboratory of Novel Thin-Film Solar Cells
North China Electric Power University
Beijing 102206, P. R. China

DOI: 10.1002/adfm.201502224

spheres with the optimum parameters to meet the above requirements. Based on these parameters, the different porosities of microspheres are prepared by adjusting the amount of ethanol. In the second part, we have studied the effect of different porosities on the performance of the DSSCs and their properties including dye loading, electrolyte diffusion, and electron collection. We found that the large porosity of microspheres possesses an abundant dye adsorption, rapid dye regeneration, and sufficient electrolyte diffusion, resulting in a high short-circuit current density (J_{sc}) and a high power conversion efficiency (PCE) (η). Finally, further optimizing the TiO_2 microsphere film results in an efficiency of 11.67%, which is greater higher than 9.94% of nanoparticle-based film with similar film thickness.

2. Results and Discussions

2.1. Synthesis and Materials Characterization

2.1.1. Effects of the H_2O:Ti Volume Ratio

TiO_2 microspheres were synthesized via sol–gel methods. The hydrolysis and condensation reactions are concerned with this sol–gel process.[4] After the reaction, spherical microspheres which are amorphous structure and have a smooth surface can be generated (Figure S1, Supporting Information). The final diameter of microspheres is determined in this process. The amount of H_2O (including the 0.1 M potassium iodide (KI) aqueous) in the sol–gel process plays a vital role in the diameter of microspheres. **Figure 1** shows scanning electron microscopy (SEM) images of the TiO_2 microspheres obtained with decreasing H_2O to Ti volume ratios from 3:10, 1:4, to 1:5. When the volume ratio is 3:10, the microspheres are monodisperse, and at this ratio the diameter is 300 ± 40 nm (MS300, Figure 1a,b). A portion of microspheres is not quite spherical. If the volume ratio is further increasing, the diameter of microspheres substantially decreases and the morphology is subjected to distorted spherical structure. Decreasing the H_2O content results in an increase in the diameter of the microspheres, with a diameter of 500 ± 60 nm (MS500, Figure 1c,d). The decreased H_2O content restrains the hydrolysis reaction of titanium (IV) isopropoxide (TTIP), which decreases the number of nuclei and thereby accelerates the growth of individual microspheres.[15] Therefore, 800 ± 100 nm microspheres (MS800) are formed at the volume ratio of 1:5 (Figure 1e,f). The overall monodispersity of microspheres is not appreciably changed, but they are still not uniform.

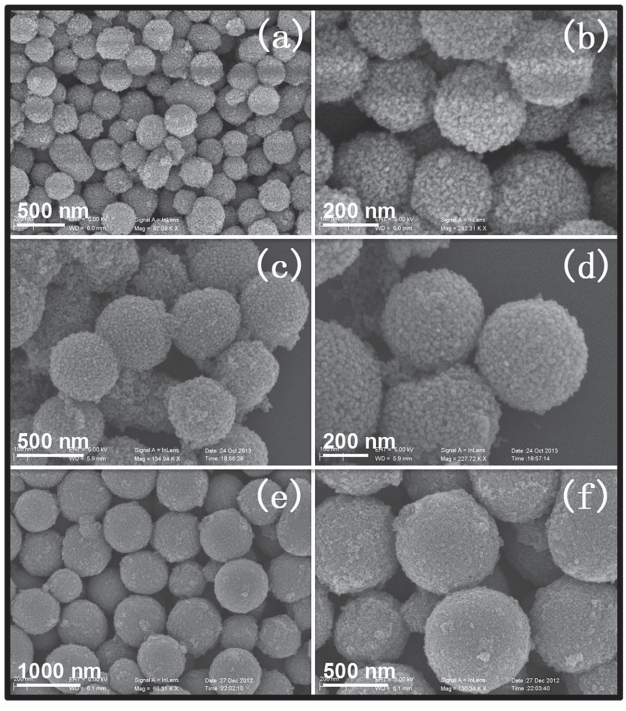

Figure 1. SEM images of TiO_2 microspheres synthesized with varying H_2O:Ti volume ratios: a,b) 3:10, c,d) 1:4, and e,f) 1:5. Note: All of these SEM images were obtained without Au sputter coating of the samples.

Specific surface area and average pore size are measured by using N_2 adsorption–desorption experiments with the samples after sintering the pastes (Figure S2, Supporting Information), and the results are shown in Table S1 (Supporting Information). Although the microspheres have different diameters, they have similar surface areas and average pore sizes. This phenomenon is in accordance with the results reported by Chen.[9] They found that the 550 ± 50 nm beads show the best light-scattering properties than those of 320 ± 50 and 830 ± 40 nm beads in the wavelength region from 400 to 800 nm. Therefore, we choose the MS500 microspheres as the research object in this work.

2.1.2. Effects of Ammonia

By way of the solvothermal reaction at 200 °C for 16 h instead of the conventional calcination process, the amorphous microspheres are converted into a crystallized structure.[16] **Figure 2**a–e shows SEM images of TiO_2 microspheres after solvothermal treatment with 0, 0.25, 0.50, 0.75, and 1.0 mL ammonia (Named: MS500A, MS500B, MS500C, MS500D, and MS500E, respectively). The MS500A microspheres are composed of interconnected TiO_2 tiny nanocrystals. With increasing ammonia volume, the nanocrystals at the surface of the microspheres grow larger. It is noteworthy that ammonia serves as an accelerator to reduce the solubility of the hydroxide precipitate in ethanol because it forms ammonia complexes in water through its coordination to the Ti ion, which inversely increases the solubility of the precipitate and enhances the crystal growth.[16] Confirmed by X-ray diffraction (XRD) (Figure 2f), the diffraction peaks become sharper with increasing the amount of ammonia, along with the growth of crystals. As shown in Figure S3 (Supporting Information), Type IV isotherms and H1 type hysteresis loops are observed in the five microspheres, indicating their relatively large mesopores. The surface areas and average pore sizes are summarized in the Table S2 (Supporting Information). As the pore size of the microspheres increases along with an increase in crystallite, there is a constant decrease in surface area. Among these microspheres, from the point of surface area and pore size, the MS500C microspheres are chosen as the most appropriate sample for preparing photoanode in DSSCs.

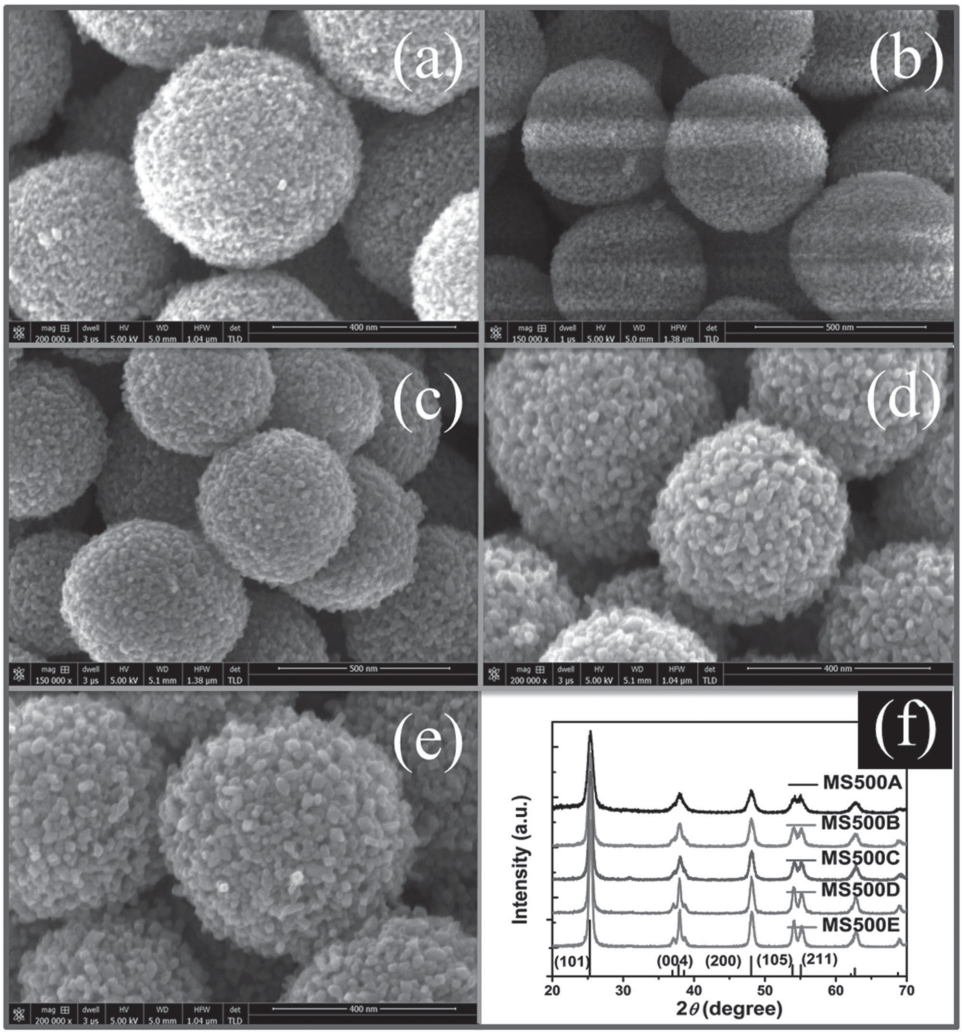

Figure 2. SEM images of TiO_2 microspheres synthesized with different contents of ammonia: a) 0 mL, b) 0.25 mL, c) 0.50 mL, d) 0.75 mL, and e) 1.00 mL. f) The corresponding XRD patterns of the TiO_2 microspheres. Note: All of these SEM images were obtained without Au sputter coating of the samples.

2.1.3. Effects of the Amount of Ethanol

According to the above analysis, the physical parameters of microspheres are fixed in a diameter of 500 ± 60 nm with surface area of ≈120 m^2 g^{-1} and average pore size of ≈12 nm. In the sol–gel process, the amount of ethanol has an obvious effect on the porosity of microspheres.[17] SEM images in **Figure 3** show morphologies of the microspheres synthesized in the three contents of ethanol. All microspheres show the similar surface morphology. Whereas, the interior structure of microspheres are of significant difference observed by the transmission electron microscopy (TEM) images.

As seen in **Figure 4**a, the microspheres composed of nanocrystals are solid and monodispersed. When the ethanol:Ti volume ratio is 25:1 (MS500C-L, Figure 4b), the abundant disordered mesopores (internal pores) are existed in the interior structure of microspheres. The microspheres are gradually dense with increasing the ratio from 100:3 (MS500C-M, Figure 4c) to 50:1 (MS500C-D, Figure 4d). The microspheres of

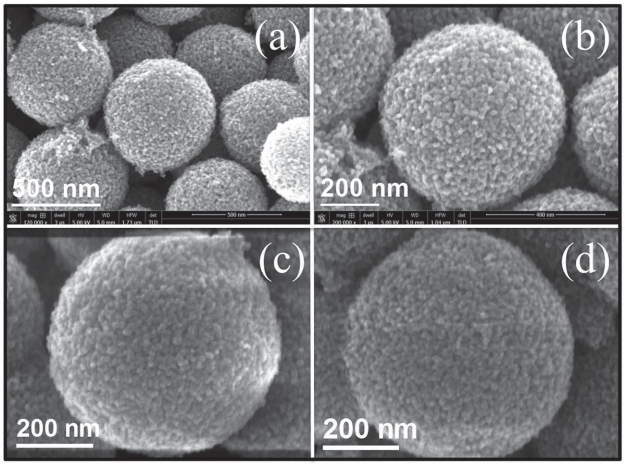

Figure 3. SEM images of TiO_2 microspheres synthesized with varying ethanol:Ti volume ratios: a,b) 25:1, c) 100:3, and d) 50:1. Note: All of these SEM images were obtained without Au sputter coating of the samples.

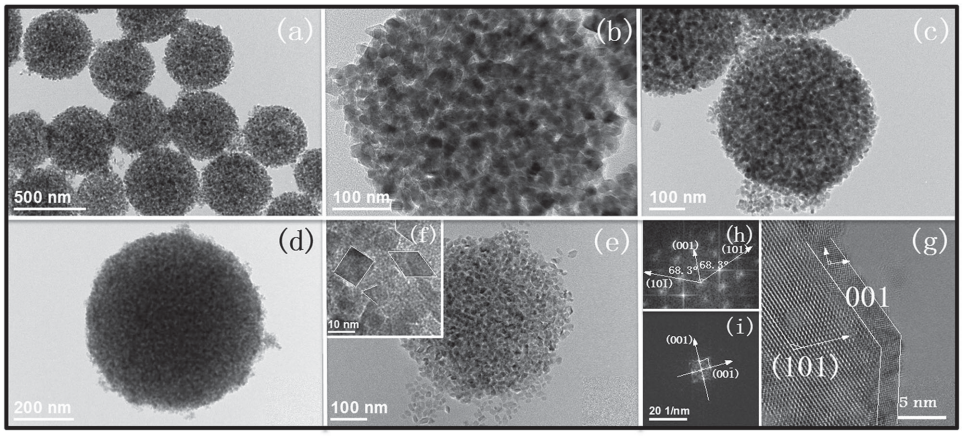

Figure 4. TEM images of TiO_2 microspheres synthesized with varying ethanol:Ti volume ratios: a,b) 25:1, c) 100:3, and d) 50:1. e) TEM image of the ultramicrotomed MS500C-D microspheres and f) enlarged image of the nanocrystals. g) High-resolution TEM image of the intergrowth of the nanocrystals within the microspheres, as indicated by the write parallel lines. h,i) Images of the FFT patterns with the lattice planes (101) and (001).

MS500C-D are cut to ≈60 nm thickness by the ultromicrotomy technique to investigate the interior structure and crystal intergrowth (Figure 4e). The ultramicrotomed TEM image shows the interior structure packed with nanocrystals is densely compact and has less mesopores, indicating that it is difficult to adsorb dyes and diffuse electrolytes in the DSSCs.[10,13] The high-resolution TEM in Figure 4f indicates that the nanocrystals with a size ≈12 nm are irregular diamond shaped, in a good agreement with that calculated from XRD pattern. It is interesting to see that the nanocrystals in Figure 4g have a faceted shape. The faceted surfaces are identified as (101) and (001) planes by comparative analysis of the lattice spacings and interfacial angles in the fast Fourier transform (FFT) pattern (Figure 4h,i).[18] Thus, the high crystalline microspheres applied into the DSSCs are expected to be responsible for the reduced recombination and extended electron lifetime.

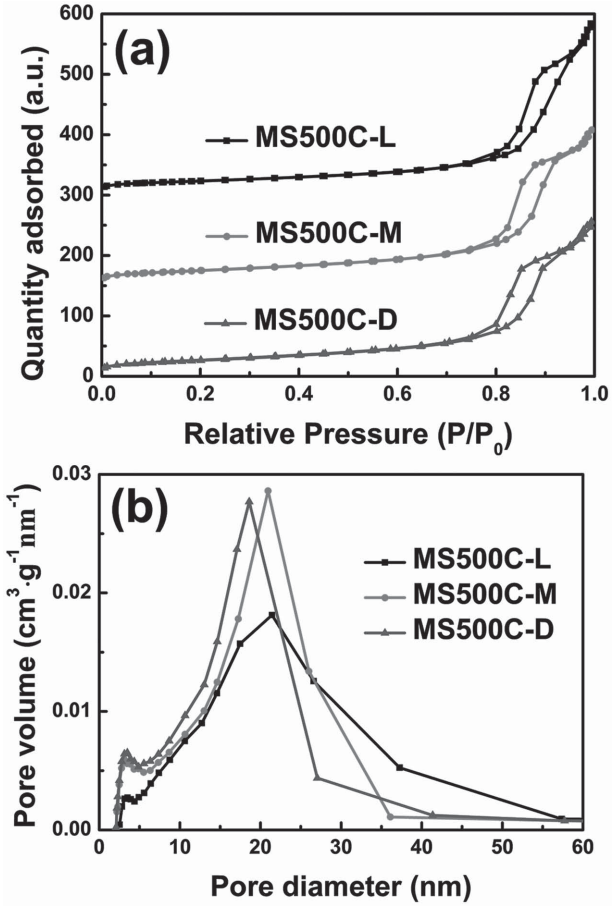

Figure 5. a) N_2 adsorption/desorption isotherms and b) corresponding pore size distributions of the microspheres with different porosities after calcination.

The XRD patterns in Figure S4 (Supporting Information) indicate that all of the microspheres are indexed into the pure anatase phase. Besides, according to the Scherrer equation, the crystallite sizes are not appreciably affected by varying the amount of the ethanol. Larger mesopores are existed in the MS500C-L microspheres than those of the other two microspheres, authenticated by a sharper capillary condensation step and a H1-type hysteresis loop at higher pressure in the type IV isotherm (**Figure 5**). The crystallite sizes, physical characteristics and dye surface concentration are illustrated in the **Table 1**. The pore size decreases from 22.7 to 16.9 nm with increasing the amount of ethanol, corresponding to the decrease of porosity

Table 1. Physical properties of the three microspheres with different crystallite sizes after calcination.

Samples	Crystallite size[a)] [nm]	Pore size [nm]	Porosity[b)] [P]	S_{BET} [$m^2\ g^{-1}$]	Roughness factor[c)]
MS500C-L	14.6	22.7	0.602	98.2	152
MS500C-M	15.0	19.4	0.585	94.3	152
MS500C-D	15.1	16.9	0.551	89.7	157

[a)]Crystallite sizes are calculated by the Scherrer equation to the (101) anatase peak; [b)]Porosity is measured from the Barrett-Joyner-Halenda (BJH) pore volume according to $P = \rho V_p / (1 + \rho V_p)$; [c)]Roughness factor = $\rho \times (1 - P) \times S_{BET}$, where ρ was taken as 3.893 g cm^{-3}.

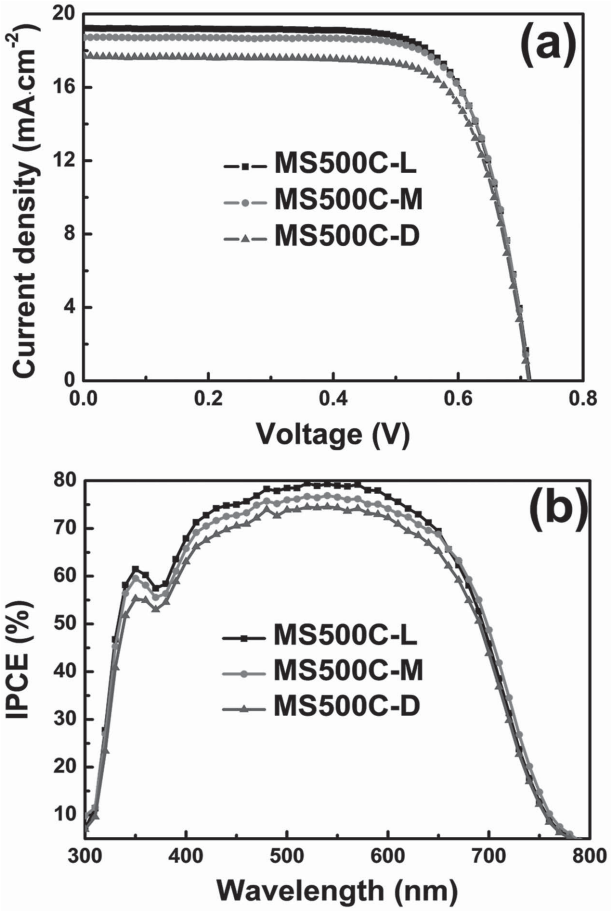

Figure 6. a) *J–V* curves and b) IPCE spectra of MS500C-L-, MS500C-M-, and MS500C-D-based DSSCs.

from 0.602 to 0.551. Thus these microspheres are ideal for investigating the effect of pore size and porosity on the diffusion of redox couple and the photovoltaic performance of DSSCs.

2.2. Photovoltaic Performances of DSSCs

Current density–voltage (*J–V*, **Figure 6**a) characteristics of films made up with the three TiO_2 microspheres were measured under illumination of AM1.5 simulated sunlight and are summarized in **Table 2**. The three DSSCs possess the similar open-circuit voltage (V_{oc}) and fill factor (FF). The slight decrease in V_{oc} would be illustrated later. Whereas, it is notable that the MS500C-L microspheres-based DSSC shows a short-circuit current density (J_{sc}) of 19.21 mA cm^{-2} and an overall power conversion efficiency (η) of 9.98%. The performance of MS500C-L is better than that of the MS500C-M and MS500C-D with moderate η of 9.86% and 9.29%, respectively. The improved η mainly rests with the higher J_{sc} of the former than the latter two (19.21 mA cm^{-2} vs 18.73 and 17.69 mA cm^{-2}).[19] The inherent reasons for J_{sc} improvements will be explained by incident photon-to-current conversion efficiency (IPCE, Figure 6b), according to the follow equation:

$$J_{sc} = q \times \mathrm{IPCE}(\lambda) \times I_0 \quad (1)$$

$$\mathrm{IPCE}(\lambda) = \mathrm{LHE}(\lambda)\varphi_{inj}\eta_c \quad (2)$$

where q is elementary charge, I_0 is light intensity, LHE(λ) is light harvesting efficiency, φ_{inj} is electron injection efficiency, and η_c is electron collection efficiency.[20,21]

2.3. Dye Adsorption and Electrolyte Diffusion Analysis

Firstly, φ_{inj} can be ignored resulting from the identical dye sensitized onto TiO_2 microspheres. Then, the LHE(λ) is mostly decided by the dye loading and light scattering of photoanodes. As reflected by the diffused reflectance spectrum shown in the Figure S5 (Supporting Information), the three photoanodes are provided with the similar light scattering capability, resulting from the same diameters of microspheres. **Figure 7** shows the TEM elemental mappings of dye-sensitized TiO_2 microspheres. The results show that the S atoms consisted in the C101 dye (Figure 7e) are not intensively distributed in the edge of microspheres, but homogenously coated onto the microsphere structures. This phenomenon verifies that the dye can diffuse into the interior structure of microspheres through the mesopores. Therefore, the pore size and porosity play important roles in the dye loading.[10,13]

Dye loading on the three microspheres measured after desorbing the dyes is reported in Table 2. For the same film thickness, the amount of dye loading on MS500C-L is 117% of what is adsorbed on MS500C-D, despite very similar surface areas (Table 1). Indeed, taking into consideration the relationship between the porosity and dye loading of the film, the same proportionality is kept for the three microspheres, indicating that the internal surface is actually accessible to dye molecules. Besides, the large mesopores can provide facile channels for the efficient diffusion of dye.[10,13]

Figure 8 shows three hemispheres in the Nyquist plots for three DSSCs measured by electrochemical impedance spectroscopy (EIS). In general, three hemispheres can be recognized and fitted according to an equivalent circuit. The high-frequency region (10^4–10^2 Hz), intermediate frequencies (10^2–10 Hz), and low frequency region (10–0.01 Hz), respectively, represent the interface of Pt/FTO, dyed-TiO_2/electrolyte,

Table 2. Photovoltaic characteristics and dye adsorption parameters of MS500C-L-, MS500C-M-, and MS500C-D-based DSSCs.

Cell	V_{oc} [V]	J_{sc} [mA cm^{-2}]	FF	η [%]	Dye loading [$\times 10^{-8}$ mol cm^{-2} μm^{-1}]	Dye surface concentration[a)] [$\times 10^{-11}$ mol cm^{-2}]
MS500C-L	0.715	19.21	0.726	9.98	1.569	10.3
MS500C-M	0.714	18.73	0.738	9.86	1.491	9.8
MS500C-D	0.712	17.69	0.730	9.29	1.342	8.5

[a)]Dye surface concentration = dye loading/roughness factor.

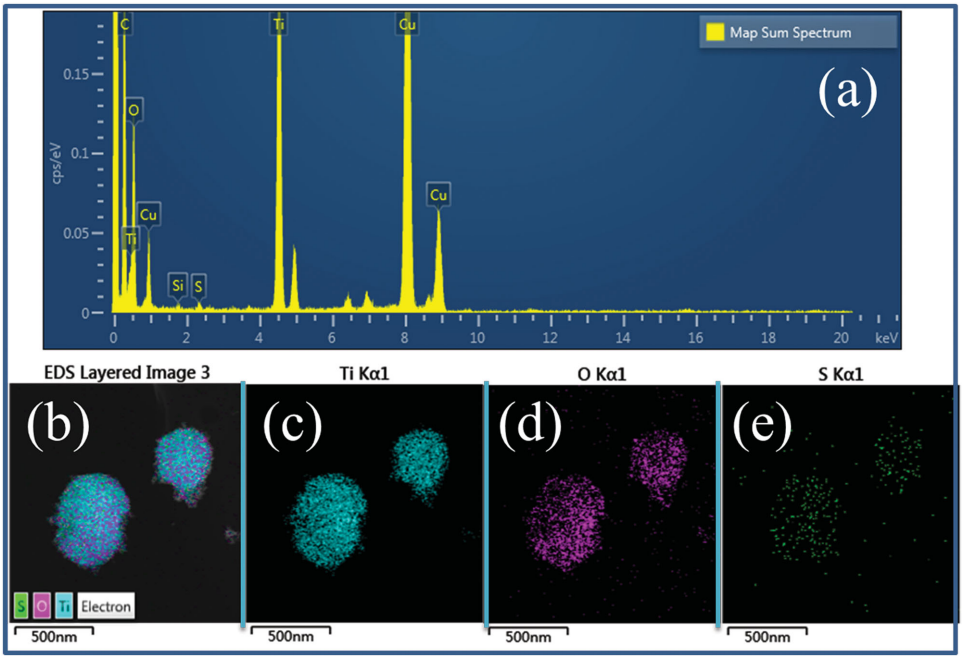

Figure 7. a) TEM mapping sum spectrum and elemental mapping for b) sum, c) Ti, d) O, and e) S atoms of MS500C-D microspheres.

and the Nernst diffusion of the electrolyte.[12] The fitted data are listed in **Table 3**. By comparison the diffusion resistance (R_{Diff}) of the electrolyte for each DSSC, we find the MS500C-L shows an appreciable lower R_{Diff} compared to that of the MS500C-M and MS500C-D. This suggests that the MS500C-L, possessing a high porosity and large mesopores, induces relatively more efficient diffusion of I_3^-/I^-. The values of electron lifetime ($\tau_{n(EIS)}$) are determined by the electron transfer resistance (R_{ct}) and chemical capacitance (CPE2) simultaneously. According to the relationship: $\tau_{n(EIS)} = R_{ct} \times CPE2$,[20] the $\tau_{n(EIS)}$ is higher (168.7 ms) in the photoanode with the MS500C-L, indicating less recombination occurring at the dyed-TiO_2/electrolyte interface, hence resulting in a higher V_{oc}. Additionally, the $\tau_{n(EIS)}$ shows a decreasing trend as MS500C-D < MS500C-M < MS500C-L. As discussed above, the diffusion of I_3^-/I^- is a serious problem for photoanode with a low porosity and small mesopores, which would restrain the dye regeneration.[12] Beyond that there is an increase in the risk of recombination between injected electrons in the conduction of TiO_2 microspheres and I_3^- in the electrolyte because of the slow transport of I_3^-/I^- near TiO_2 microspheres surface.[10]

The regularity of the electron lifetime (τ_n) is also confirmed by the intensity modulated photovoltage spectroscopy (IMVS) measurements (Figure S6, Supporting Information).[22] Whereas, the electron transport time (τ_d) measured by the intensity modulated photocurrent spectroscopy (IMPS) are similar, since the nanocrystals making up microspheres structure are densely interconnected to one another.[2] Combining τ_d together with τ_n allows us to view the electron collection efficiency (η_c) of the three photoanodes, calculated by the equation $\eta_c = 1 - \tau_d/\tau_n$. Their η_c are in the sequence of MS500C-D > MS500C-M > MS500C-L, which is basically in conformity to

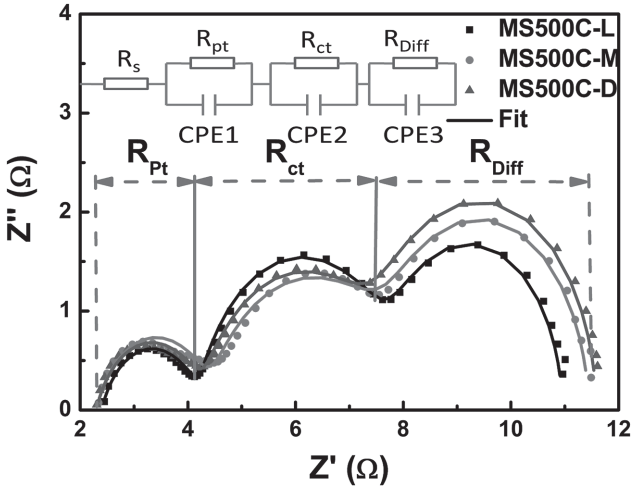

Figure 8. a) Nyquist impedance plots of the three photoanodes for DSSCs. Experimental data are represented by dots and solid lines correspond to fitted data. The inset shows the electrical elements of the equivalent circuit in the DSSC.

Table 3. Fitting results of EIS parameters for the DSSCs based on the three porosities of the microspheres.

Cells	R_s[a)] [Ω]	R_{pt}[b)] [Ω]	R_{ct} [Ω]	CPE2 [mF]	$\tau_{n(EIS)}$ [ms]	R_{Diff} [Ω]
MS500C-L	2.4	3.6	3.13	53.9	168.7	1.81
MS500C-M	2.3	3.39	3.93	38.9	152.9	1.97
MS500C-D	2.3	3.43	3.60	40.7	146.5	2.12

[a)] R_s is the series resistance; [b)] R_{pt} represents the charge-transfer resistance at the Pt counter electrolyte/electrolyte interface.

their porosity sequence. By comprehensive review of LHE(λ) and η_c sequences for the three photoanodes, there is undoubtedly on the IPCE sequence of MS500C-D > MS500C-M > MS500C-L.

The photoinduced charge (Q) in the TiO_2 microspheres photoanodes was also calculated by the IMVS/IMPS measurements. The V_{oc} as a function of ln$Q$ in the DSSCs is shown in Figure S7 (Supporting Information). According to the relationship: $V_{oc} = V_c + m_c\ln(Q)$, there is a direct linear relationship between the V_{oc} and Q.[23] For a given Q, the decrease in V_{oc} is ascribed to a downward shift of the TiO_2 conduction band edge. Hence, the conduction band edges of the photoanode in the DSSCs with MS500C-L are more positive than those with MS500C-M and MS500C-D, resulting from the higher dye surface concentration (10.3×10^{-11} mol cm^{-2} vs 9.8×10^{-11} and 8.5×10^{-11} mol cm^{-2} in the Table 2).[8,11,24] Generally, the positive shift of the TiO_2 conduction edge leads to decrease in V_{oc}, which would offset the increase of V_{oc} in less electron recombination. Therefore, the V_{oc} is slightly decreased as a whole.

TiO_2 microspheres with high porosity and large mesopores have great advantages for preparing high efficient DSSCs. Preliminary experiments show that the η is improved by adopting the nanocrystalline layer as a bridge to link the microspheres and substrate, and constructing the continuous electron transport pathway via adding nanocrystallines into microspheres.[25] By optimizing the microsphere interconnection and external pores, we have yielded 20.23 mA cm^{-2} of J_{sc} and 11.67% of η, significantly higher than that derived from nanoparticle photoanode of similar thickness (Figure S8, Supporting Information).

3. Conclusions

TiO_2 microspheres with tunable diameter, pore size, and porosity were synthesized by changing the experimental conditions, such as the ratio of deionized water, ammonia, and ethanol, respectively. Through comparative analysis of light scattering, specific surface area, and pore size, microspheres with the favored parameters (500 nm in diameter, 16 nm of pore size, and high porosity) were chosen as photoanode material for DSSCs. Based on these parameters, we have studied the effect of porosity on the dye loading, regeneration, and electrolyte diffusion, along with the photovoltaic performance of DSSCs. As confirmed by the TEM elemental mapping and dye loading ability, the TiO_2 microspheres with large pore size and high porosity provide a high internal surface area for dye adsorption, giving rise to high light harvesting. In addition, EIS measurements revealed that a high porosity in the microspheres offers a pathway for unhindered electrolyte diffusion, resulting in high electron collection efficiency. Consequently, the highest photocurrent of 19.21 mA cm^{-2} and a PCE of 9.98% were obtained by using the TiO_2 microspheres with the highest porosity, compared with 9.29% efficiency demonstrated by the lowest porosity (an improvement of 7.4%). Finally, a high efficiency of 11.67% has been achieved for a DSSC based on the optimal TiO_2 microspheres by modifying the microsphere interconnection and external pores. Therefore, these parameters are both critical for the future preparation of high-efficiency DSSCs with TiO_2 microspheres as photoanodes.

4. Experimental Section

Chemicals: TTIP (97%) and KI were purchased from Sigma-Aldrich. Absolute ethanol (AR) and ammonia solution (28 wt%) were used for the synthesis without further purification.

TiO_2 Microspheres Preparation: TiO_2 microspheres were synthesized by a two-step process of controlled hydrolysis and a subsequent hydrothermal reaction. First, the amorphous microspheres are prepared via a sol–gel process with a certain amount of KI (0.1 M) to adjust the ionic strength of the solution. The solution composition of TTIP:H_2O:KI:ethanol (volume ratio) was varied in the range of 1.0:(0.1–0.15):(0.1–0.15):(25–50). Second, the as-obtained precipitates were in the amorphous phase, and their surfaces were smooth without any pores. After the subsequent solvothermal process at 200 °C for 16 h, the amorphous microspheres were crystallized with a little of ammonium hydroxide (0–1.0 mL) to promote the growth rate of TiO_2 crystallization. In a typical synthesis, 60 mL of TTIP was dropwise added into the mixture of ethanol (2.5 L), deionized water (7.5 mL), and KI solution (7.5 mL) to obtain a milky white precursor under magnetic stirring. Such precursor suspension was kept static for 24 h and then centrifuged, and the precipitate was washed with ethanol three times and dried in 30 °C. The amorphous precursor microspheres (2.5 g) were dispersed in a mixture of 40 mL ethanol and 20 mL H_2O with ammonia of 0.5 mL. Then the resulting mixtures were transferred into a Teflon-lined autoclave (100 mL) and heated at 200 °C for 16 h. After washing with water and ethanol, the crystallographic TiO_2 microspheres were collected and dried for characterization.

Fabrication of DSSCs: Those crystallographic microspheres (5.0 g) were redispersed in the ethanol suspension, containing 1.0 g ethyl cellulose and 25.0 g α-terpineol similar with the previously reported procedure.[26] The TiO_2 pastes were prepared by using rotary evaporation to remove the more volatile ethanol solvent. The as-prepared pastes were screen printed onto the F-doped tin oxide glass (FTO, 15 Ω sq^{-1}) and then sintered in air at 510 °C for 30 min. The thickness of the films was measured by a profilometer (XP-2, AMBIOS Technology, Inc., USA). The five freshly TiO_2 photoanodes were soaked into 0.1 M $TiCl_4$ aqueous solution and stored in a closed container at 65 °C for 40 min. Those films were sintered again after washing with deionized water. Then, those photoanodes were immersed into a 300×10^{-6} M C101 dye with cheno-3a, 7a-dihydroxy-5b-cholic acid for the whole night. After being washed by acetonitrile and dried in air, the sensitized photoanodes were assembled with the Pt-modified counter electrode and high-efficiency electrolyte (30×10^{-3} M I_2, 50×10^{-3} M LiI, 1 M 1,3-dimethylimidazolium iodide, 0.5 M *tert*-butylpyridine, and 0.1 M guanidinium thiocyanate (GuSCN) in a solvent mixture of 85% acetonitrile with 15% valeronitrile by volume) by a laser engraved 60 μm Surlyn gasket under heat and pressure.

Characterization: The morphologies of the TiO_2 microspheres were seen by a SEM (S-4800, HITACHI, Japan). Field emission transmission electron microscopy (FE-TEM) was performed on a JEM-2100F transmission electron microscope with accelerating voltage of 200 kV. The microspheres were ultramicrotomed to ≈60 nm thickness to investigate the interior structure and crystal intergrowth. The composition and crystal structure of the products were analyzed by XRD (MXPAHF, Mark Corp., Japan) with a scanning rate of 10° min^{-1} in the 2θ from 20° to 70° and calculated the crystallite size based on the Scherrer equation. X-ray photoelectron spectroscopy (ESCALAB 250, Thermo Scientific) was used to determine the chemical composition of the powders with calibration of C 1s peak (284.6 eV). The Brunauer–Emmett–Teller (BET) surface area and pore size distribution of the microspheres were evaluated by using a micromeritics (TriStar II 3020 V1.03, Micromeritics Instrument Corporation) nitrogen adsorption/desorption apparatus. UV–vis diffuse reflection spectra and absorption spectra were obtained from a UV–vis spectrophotometer (SOLID 3700, Shimadzu Co. Ltd, Japan) to measure the diffuse reflectance of films and dye amounts detached from films, respectively.

The current density–voltage (J–V) measurements were carried out on a Keithley model 2420 digital source meter controlled by Test

point software under a xenon lamp (100 mW cm^{-2}). The active area of photoanodes was 0.25 cm^{-2}. The IPCE values were confirmed as a function of wavelength from 300 to 800 nm (PV Measurements, Inc.) for DSSCs. An electrochemical workstation (IM6e, Zahner, Germany) was conducted to measure the intensity of the modulated photocurrent/photovoltage spectroscopy (IMPS/IMVS) with light emitting diodes (LED, $\lambda = 610$ nm) driven by Export (Zahner, Germany). Small amplitude is 10% or less than that of the dc component provided by the LED, and the frequency range was from 300 mHz to 3 kHz. The electrochemical impedance spectra (EIS) were recorded by a computer controlled potentiostat (Autolab 320, Metrohm, Switzerland) in a frequency range of 10 mHz–1000 kHz applied in the dark.

Supporting Information

Supporting Information is available from the Wiley Online Library or from the author.

Acknowledgements

This work was supported by the National Natural Science Foundation of China (Grant Nos. 21173228 and 61404142), the National High Technology Research and Development Program of China (Grant No. 2015AA050602), and the China Postdoctoral Science Foundation (Grant No. 2014M551825).

Received: June 1, 2015
Revised: July 12, 2015
Published online: August 26, 2015

[1] a) B. Oregan, M. Grätzel, *Nature* **1991**, *353*, 737; b) M. Grätzel, *Nature* **1991**, *349*, 740.
[2] F. Sauvage, D. Chen, P. Comte, F. Huang, L. P. Heiniger, Y. B. Cheng, R. A. Caruso, M. Graetzel, *ACS Nano* **2010**, *4*, 4420.
[3] a) W. Q. Wu, Y. F. Xu, H. S. Rao, C. Y. Su, D. B. Kuang, *J. Am. Chem. Soc.* **2014**, *136*, 6437; b) W. Q. Wu, Y. F. Xu, H. S. Rao, H. L. Feng, C. Y. Su, D. B. Kuang, *Angew. Chem. Int. Ed.* **2014**, *53*, 4816.
[4] D. Chen, L. Cao, F. Huang, P. Imperia, Y. B. Cheng, R. A. Caruso, *J. Am. Chem. Soc.* **2010**, *132*, 4438.
[5] D. Chen, R. A. Caruso, *Adv. Funct. Mater.* **2013**, *23*, 1356.
[6] X. W. Lou, L. A. Archer, Z. Yang, *Adv. Mater.* **2008**, *20*, 3987.
[7] a) F. Huang, D. Chen, X. L. Zhang, R. A. Caruso, Y.-B. Cheng, *Adv. Funct. Mater.* **2010**, *20*, 1301; b) S. H. Hwang, J. Yun, J. Jang, *Adv. Funct. Mater.* **2014**, *24*, 7619; c) D. Chen, F. Huang, Y.-B. Cheng, R. A. Caruso, *Adv. Mater.* **2009**, *21*, 2206.
[8] I. G. Yu, Y. J. Kim, H. J. Kim, C. Lee, W. I. Lee, *J. Mater. Chem.* **2011**, *21*, 532.
[9] Y. Chen, F. Z. Huang, D. H. Chen, L. Cao, X. L. Zhang, R. A. Caruso, Y. B. Cheng, *ChemSusChem* **2011**, *4*, 1498.
[10] Y. Chen, F. Z. Huang, W. C. Xiang, D. H. Chen, L. Cao, L. Spiccia, R. A. Caruso, Y. B. Cheng, *Nanoscale* **2014**, *6*, 13787.
[11] Y. J. Kim, M. H. Lee, H. J. Kim, G. Lim, Y. S. Choi, N.-G. Park, K. Kim, W. I. Lee, *Adv. Mater.* **2009**, *21*, 3668.
[12] K. Yan, Y. Qiu, W. Chen, M. Zhang, S. Yang, *Energy Environ. Sci.* **2011**, *4*, 2168.
[13] L.-P. Heiniger, F. Giordano, T. Moehl, M. Grätzel, *Adv. Energy Mater.* **2014**, *4*, 168.
[14] a) H. S. Kim, S. B. Ko, I. H. Jang, N. G. Park, *Chem. Commun.* **2011**, *47*, 12637; b) H. N. Tsao, P. Comte, C. Y. Yi, M. Grätzel, *ChemPhysChem* **2012**, *13*, 2976.
[15] T. Kojima, T. Sugimoto, *J. Phys. Chem. C* **2008**, *112*, 18445.
[16] T. Sugimoto, T. Kojima, *J. Phys. Chem. C* **2008**, *112*, 18760.
[17] T. Sugimoto, T. Kojima, *J. Phys. Chem. C* **2008**, *112*, 18437.
[18] J. Li, Y. Yu, Q. Chen, J. Li, D. Xu, *Cryst. Growth Des.* **2010**, *10*, 2111.
[19] A. Yella, H. W. Lee, H. N. Tsao, C. Y. Yi, A. K. Chandiran, *Science* **2011**, *334*, 1203.
[20] K. Zhu, N. R. Neale, A. Miedaner, A. J. Frank, *Nano Lett.* **2007**, *7*, 69.
[21] J.-Y. Liao, B.-X. Lei, D.-B. Kuang, C.-Y. Su, *Energy Environ. Sci.* **2011**, *4*, 4079.
[22] T. Oekermann, D. Zhang, T. Yoshida, H. Minoura, *J. Phys. Chem. B* **2004**, *108*, 2227.
[23] G. Schlichthorl, S. Y. Huang, J. Sprague, A. J. Frank, *J. Phys. Chem. B* **1997**, *101*, 8141.
[24] M. K. Nazeeruddin, R. Humphry-Baker, P. Liska, M. Grätzel, *J. Phys. Chem. B* **2003**, *107*, 8981.
[25] a) Y. Ding, L.-E. Mo, L. Tao, Y.-M. Ma, L.-H. Hu, Y. Huang, X.-Q. Fang, J.-X. Yao, X.-W. Xi, S.-Y. Dai, *J. Power Sources* **2014**, *272*, 1046; b) Y. Ding, Y.-M. Ma, L. Tao, L.-H. Hu, G. Li, L. Jiang, Z.-Q Li, L.-E. Mo, J.-X. Yao, S.-Y. Dai, *RSC Adv.* **2015**, *5*, 17493.
[26] L. H. Hu, S. Y. Dai, J. Weng, S. F. Xiao, Y. F. Sui, Y. Huang, S. H. Chen, F. T. Kong, X. Pan, L. Y. Liang, K. J. Wang, *J. Phys. Chem. B* **2007**, *111*, 35.